BB

PAUL SCHERRER INSTITUT

PSI PR-95-27
December 1995

SW9606

Contribution of Initial State Interactions to the Three-Nucleon Absorption of Pions by ^{3}He

G. Backenstoss[a], D. Bosnar[i], H. Breuer[d], H. Döbbeling[h], T. Dooling[g], M. Furić[i], P. A. M. Gram[c], N. K. Gregory[e], A. Hoffart[b,h], C. H. Q. Ingram[h], A. Klein[g], K. Koch[h], J. Köhler[a], B. Kotlínski[h], M. Kroedel[a], G. Kyle[f], A. Lehmann[a], A. O. Mateos[e], K. Michaelian[h], T. Petković[i], R. P. Redwine[e], D. Rowntree[e], U. Sennhauser[h], N. Šimišević[e], R. Trezeciak[b], H. Ullrich[b], M. Wang[f], M. H. Wang[f], H. J. Weyer[a,h], M. Wildi[a], K. E. Wilson[e]

a University of Basel, CH-4056 Basel, Switzerland
b University of Karlsruhe, D-7500 Karlsruhe, Germany
c LAMPF, Los Alamos NM 87545, USA
d University of Maryland, College Park, MD 20742, USA
e Massachusetts Institute of Technology, Cambridge MA 02139, USA
f New Mexico State University, Las Cruces NM 88003, USA
g Old Dominion University, Norfolk VA 23529, USA
h Paul Scherrer Institut, CH-5232 Villigen PSI, Switzerland
i University of Zagreb, HR-41001 Zagreb, Croatia

Paul Scherrer Institut
CH - 5232 Villigen PSI
Telefon 056 310 21 11
Telefax 056 310 21 99

Contribution of Initial State Interactions to the Three-Nucleon Absorption of Pions by ^{3}He

G. Backenstoss,[a] D. Bosnar,[i] H. Breuer,[d] H. Döbbeling,[h] T. Dooling,[g] M. Furić,[i] P.A.M. Gram,[c] N.K. Gregory,[e] A. Hoffart,[b,h] C.H.Q. Ingram,[h] A. Klein,[g] K. Koch,[h] J. Köhler,[a] B. Kotlínski,[h] M. Kroedel,[a] G. Kyle,[f] A. Lehmann,[a] A.O. Mateos,[e] K. Michaelian,[h] T. Petković,[i] R.P. Redwine,[e] D. Rowntree,[e] U. Sennhauser,[h] N. Šimičević,[e] R. Trezeciak,[b] H. Ullrich,[b] M. Wang,[f] M.H. Wang,[f] H.J. Weyer,[a,h] M. Wildi,[a] K.E. Wilson[e]

(LADS collaboration)

[a] University of Basel, CH-4056 Basel, Switzerland
[b] University of Karlsruhe, D-7500 Karlsruhe, Germany
[c] LAMPF, Los Alamos NM 87545, USA
[d] University of Maryland, College Park MD 20742, USA
[e] Massachusetts Institute of Technology, Cambridge MA 02139, USA
[f] New Mexico State University, Las Cruces NM 88003, USA
[g] Old Dominion University, Norfolk VA 23529, USA
[h] Paul Scherrer Institute, CH-5232 Villigen PSI, Switzerland
[i] University of Zagreb, HR-41001 Zagreb, Croatia

Abstract

The distributions of protons after the absorption of positive pions by ^{3}He at 118, 162 and 239 MeV are presented. A decomposition of the three-nucleon cross section in terms of initial state interactions and other processes is given, based upon simple models. A clear signal of initial state interactions is visible in the data, diminishing at the lower energies.

1 Introduction

Absorption is one of the major nuclear reactions of pions of up to a few hundred MeV kinetic energy. Because the pion is the lightest hadronic exchange boson, the details of the absorption dynamics could lead to new insights into the nuclear force. Absorption on two nucleons (2NA) is the main channel in light nuclei at these energies, but a significant part of the total absorption cross section leads to more than two energetic nucleons in the final state, even for ^{3}He [1]-[6]. The 2NA reaction closely follows the behaviour of the elementary absorption cross section on the deuteron. The three-nucleon absorption (3NA) distributions from ^{3}He were observed to be similar to those of three-nucleon (3N) phase space, and it was inferred that this could indicate a new reaction dynamics, although no detailed explanation is available [7, 8]. Evidence of the 3NA of photons by ^{3}He has also been reported [9]-[12].

A reaction in which the pion undergoes a quasi-free scattering on one nucleon followed by its absorption on two others could lead to three energetic final state nucleons. A similar final state could result if, after the absorption of the pion on two nucleons, one of these re-scatters off a third nucleon. In this paper we refer to these processes as initial (ISI) and final (FSI) state interactions respectively. In the case that these processes are simple and cascade-like, they might produce definite kinematic signatures in the distributions of the three final state nucleons. However, experimental searches for such signatures after pion absorption on ^{3}He have so far revealed no clear signal [5, 13].

On heavier nuclei, the observed number of nucleons emitted after pion absorption has been found to be larger than can be explained by 2NA and the effects of FSI processes [14]-[19]. Calculations [20, 21] suggesting that ISI processes could also be important have not been experimentally confirmed [22]-[25]. Thus in absorption on heavier nuclei there also appears to be an unexplained excess of reactions leading to more than two fast nucleons. However, detailed knowledge of the multi-nucleon final states, including those for reactions on ^{3}He, has been limited by the acceptance or kinematic definition of the experiments.

In this paper we present results for pion absorption on ^{3}He, measured at PSI with the Large Acceptance Detector System (LADS). The three-nucleon distributions are investigated in greater detail than has been previously possible, and significant deviations from 3N phase space are seen. Partial absorption cross sections for the data presented here were given in Ref. [6].

2 Experiment

The experiment was performed at the πM1 pion beam at the Paul Scherrer Institute. A flux of about 10^6 momentum-analysed pions per second was focussed on a 26 cm long 94 bar ^{3}He target (250 mg/cm^2) placed inside the detector. The gas was contained in a 4 cm diameter, 110 mg/cm^2 thick carbon/epoxy cylinder with a silver/copper lining. Incident pions were required to pass through a 2 cm diameter scintillator placed 50 cm upstream of the target, and a system of veto counters ensured that only one incident particle was present for accepted events. About 5% of the total incident flux satisfied these requirements. For the results presented here, incident pion energies of 118, 162 and 239 MeV were used.

The LADS detector consisted of a 28-sector cylinder of 160 cm long plastic scintillators of 30 cm inner and 68 cm outer radius, with the ends closed by 14-sector end-cap arrays, so that the solid angle covered is over 98% of 4π. The target was suspended mid-way between the two end-caps, which were 90 cm apart. Particle energies were measured by the light produced in the scintillators, whose total thickness was over 35 cm for most trajectories. Particles were identified by energy-loss and by time-of-flight, while two concentric cylindrical multi-wire proportional chambers of 6.4 and 28 cm radius provided tracking and vertex information. Further experimental details may be found elsewhere [6, 26].

3 Data analysis

The data analysis was carried out in a way which emphasised the selection of pion absorption events with a minimum of background [27]. The individual detectors' energy and time-of-flight responses were calibrated using the absorption data; in particular, to establish linear energy scales absorption events fully reconstructed kinematically from the angular information provided by the wire chambers were used. Protons were selected by a combination of cuts applied to energy-loss and time-of-flight versus total energy correlations. For all events, it was required that at least two protons be detected with hits in both wire chambers so that an interaction vertex could be reconstructed, which was required to be well within the target volume. The protons' energy losses between the vertex and the scintillators were corrected for on an event-by-event basis, using the known material along the measured tracks. The overall energy and angular resolution of the detector results in a missing mass resolution of about 8 MeV for events in which only two charged particles were detected, as shown in Fig.1.

Events in which a charged pion was detected were rejected. Detected neutral particles were ignored. To eliminate events with unidentified pions (charged or neutral) in the final state a cut on the missing mass was applied, which also removed remaining events in which protons reacted in the detector (tail to the right in Fig. 1). For events where only

two protons were detected some pionic events satisfied the missing mass requirement, and so further cuts were applied on the total detected energy; these cuts also removed a small number of absorption events.

For each event remaining after all the above selections were made, the absorption reaction kinematics was reconstructed using the two highest energy protons only. Thus in the case where the third proton was detected, that information was ignored here. This procedure was adopted in order to avoid continuity problems in threshold regions, although a few more events were lost as a result. All analysis induced losses were accounted for in the simulations described in the next section.

4 Simulations and detector acceptance

Monte Carlo simulations were made to correct for the acceptance and inefficiencies of the detector and to assist the physics interpretation of the results. Five different event generators were used to simulate: final states uniformly distributed over 3N phase space with total initial orbital angular momentum $L = 0$ and $L \geq 1$; distributions following 2NA; and distributions from ISI and FSI cascade processes. The latter processes were simulated in simple semi-classical models.

In the phase space simulations, random distributions over 3N phase space were generated. In addition, the same distribution weighted by the Legendre polynomial $P_2(cos(\xi))$ was produced, where ξ is the angle between the pion direction and the normal to the plane of the outgoing protons in the centre of mass system. Such a distribution would reflect a contribution from $L \geq 1$ states [28].

For the other simulations, the momentum distribution of the absorbing pair of nucleons was taken to be that given by a calculation [27, 29] based on ^{3}He$(e, e'$p$)$d data [30]. For the 2NA simulation, the event was weighted according to this distribution and by the differential cross section for absorption on deuterium; the latter was taken from a parameterization of experimental data [31].

For the ISI simulation, the incident pion was first scattered by one proton according to the elastic cross section [32], before being absorbed on the remaining (pn) pair according to the deuteron cross section [31]. To simulate the suppression of the forward pion quasi-elastic cross section due to the proton's binding energy, scatterings resulting in low proton momenta were suppressed by a weighting factor; this weight fell linearly from unity for 500 MeV/c protons to zero for stationary protons. For the FSI simulation, the pion was first absorbed on the (pn) pair and then one of the outgoing protons was scattered off the remaining proton according to that elastic cross section [33]; a minimum momentum transfer of 150 MeV/c was required in this case.

For all simulations, the protons were tracked through the detector, and the simulated data then reconstructed with the same analysis program as used for the real data. The effects of geometrical acceptance, energy thresholds, proton interactions in the detector and other inefficiencies and cuts were thus reflected in the proton distributions produced.

The acceptance of LADS was determined from the probability that a simulated event survived the tracking through the detector and event reconstruction. This is a function of many variables and dependent upon the full geometry of an event. Thus as a function of a single variable such as the proton angle, it is different for each of the distributions of the five simulations. To correct the measured distributions over such variables the following procedure was adopted: the distributions from the five simulations were first fitted simultaneously to the data, establishing proportions giving a good overall representation of the data. Then the acceptance over a given variable was taken to be the appropriately weighted average of the acceptances determined for each of the simulations. The distributions shown in this paper have been corrected for the acceptance in this manner.

Various checks were made to assess the reliability of the description of the acceptance in the simulations. These included checking that the effects of resolution, reaction losses, particle identification cuts and wire chamber performance were well described in the simulations, both for individual particles and for two- and three-proton distributions. The target length was about one quarter of the distance between the end-caps; comparing the acceptance-corrected cross sections from the upstream and downstream parts of the target provided a useful global check of the acceptance description, especially in the complex end-cap regions. While it is difficult to quantify how well the acceptance was described by the simulations, no substantial error was found, and in general the simulations reproduced acceptance-related features in the data well. No significant dependence of the data on the azimuthal angle ϕ was found.

Fig.2 shows the weighted acceptance as a function of proton angle. The drop in the acceptance in the forward and backward regions has two main causes. To exclude background, it was required that two protons be detected in both wire chambers, and protons in these regions did not cross the outer chamber. In addition, the highest energy protons at these angles were not be stopped in the scintillator and were lost. Events were discarded if one or more of the three protons was at an angle less than 15° or greater than 165°, where the geometrical acceptance of the detector falls rapidly to zero.

5 Results

5.1 Signature of ISI

In Fig. 3 the momentum distribution of the lowest energy final state proton is shown for each incident pion energy. The histograms are the data divided by 3N phase space. The points are the result of the 2NA simulation for 118 MeV, also divided by the 3N phase space, with the normalisation fitted to the data by the procedure described below. While the shapes of the data and the simulation agree at low momenta, substantial excess over this simulation is observed in the data at high momenta. This excess, attributed to 3NA, is similar to that observed in earlier experiments [1]-[5], although the spectra do not follow 3N phase space well (which would be a flat distribution in Fig. 3).

In order to facilitate a more detailed examination of the 3NA distributions, the requirement that each final state proton have at least 30 MeV (239 MeV/c) was imposed, which substantially removes the large yield of 2NA-plus-spectator protons which otherwise would dominate the data. The results presented in Figs 4, 5 and 6 have had this cut applied. In these figures the data have been corrected for losses due to detector efficiency and cuts applied in the analysis, including the requirement that all protons in an event lie between 15° and 165°.

In Fig. 4 the correlation between the laboratory angle and momentum for all protons is shown. A region of enhanced yield is visible at forward angles, falling in momentum as the angle increases. The curves in Fig. 4 are the kinematic trajectories corresponding to free pion-proton scattering, and it can be seen that the regions of enhanced yield are close to these lines. This suggests that the enhancements are due to the two-step ISI process where the pion first undergoes a quasi-elastic scattering on one nucleon before absorbing on the other two. The enhancement becomes less pronounced as the pion energy decreases, and at 118 MeV is barely visible.

It has been pointed out [34] that for such a two-step process, the mass squared of the intermediate state particle may be calculated, in the approximation of stationary unbound target nucleons, as $m_x^2 = (T_i + T_j)^2 - (\boldsymbol{p}_i + \boldsymbol{p}_j)^2$, where $T_{i,j}$ and $\boldsymbol{p}_{i,j}$ are the kinetic energies and momenta of two of the final state protons. Fermi motion causes the reconstructed m_x^2 peak to be broadened, but simulations indicate that a peak near the pion mass squared could still be seen. Fig. 5 shows m_x^2 spectra, calculated for all combinations of proton pairs in the data. A peak is indeed visible at a value of m_x^2 near to m_π^2 (1.9 x 10^4 MeV^2). For 118 MeV pions, the peak is reduced to a shoulder. The fits shown in Fig. 5 are discussed below. Fig. 6 shows, for 239 MeV incident pions, that the peak in m_x^2 is correlated in angle and momentum with the enhancement in Fig. 4 attributed to ISI. The contours in Fig. 6 show the areas of strong yield from 2NA in this plot if the 30 MeV proton threshold is not imposed: in particular the correlation with momentum shows that the

observed peaks in Fig. 5 are not remnants of those produced by 2NA.

Previous experiments did not reveal such a clear signature of ISI processes. In Ref. [13] an explicit search for an ISI signal was reported, for the absorption of 120 MeV pions on ^{3}He; no peak was seen in the m_x^2 plot, but this is consistent with the present result for 118 MeV (see Fig. 5), where even with full kinematic coverage the ISI signal is barely visible. Some structure may be seen in the same variable for 162 MeV incident pions in Ref. [5], but firm conclusions were not drawn. For ^{12}C, Ref. [23] reported a structure in the spectra of protons at 8° in the (π^+,3p) reaction at 240 MeV which could be an ISI signature similar to that seen in Fig. 4; its magnitude is similar to that of the ISI signal seen in this data at forward angles. A similar structure may also be visible in the data of Ref. [24].

5.2 Composition of the 3NA cross section

In order to estimate the relative strengths of different reaction processes, the results of the various simulations described above were simultaneously fitted to the data, with the normalisations of each of the simulations as the fit parameters. Because of the dominance of the 2NA yield, first a fit to the full data was made, and then a fit to the data with the 30 MeV threshold applied, but with the tail of the 2NA yield above that threshold fixed by the fit to the full data. If necessary, the procedure was iterated to achieve consistent results between the two fits.

Two sets of distributions were fitted, giving consistent results. One set was composed of the three correlations between momenta and angle of the protons and m_x^2. The second set consisted of the simple distributions over the minimum and maximum opening angles between the two protons, the plane angle, ξ, and an angle, γ, which depends on the distribution of the protons within the plane [26, 27]; these four angles, together with the physically uninteresting azimuthal plane angle, form an orthogonal set which fully describes a three-particle distribution. Fits to various other sets of distributions, and to the data with the cuts applied varied, were used as an assessment of the stability of the results. The effect of varying some of the details of the physics models, such as how binding energy effects were treated, was also investigated.

The fitted sum of the simulations is compared to the m_x^2 spectra in Fig. 5. The overall agreement is fair. Although the position and width of the peak in Fig. 5 are not perfectly reproduced by the simulations, only the ISI simulator contains this feature, and in this analysis is the only process which could produce this structure. The proton angle-momentum correlations also contain structures (including the enhancements seen in Fig. 4) which are present only in the ISI simulator; the fits to these correlations are fair. The amounts of ISI in the 3NA yield given by the fits are 13-24%, 17-26% and 27-33% at 118, 162 and 239 MeV respectively. Expressed in terms of the total absorption cross section

[6], the ISI component is 3.5-6%, 6-8.5% and 9.5-11.5% at the three energies.

The amount of FSI given by the fits was relatively less stable than the amount of ISI, as the distributions from that model are not qualitatively distinct from those of phase space. As the separation between phase space and FSI does not appear reliable, the fractions of these are not given here. However, the fits suggest that phase space describes at least half of the 3NA cross section at all three energies.

Since the simulations used in the fits are based on simple models of the physics, the results presented here should be understood as estimates of the composition of the 3NA final state. Although the amount of ISI required in the fits was quite stable with the physics models used, it should be emphasised that other models could suggest different amounts of ISI. Given the disagreements between the fits and the data, somewhat larger fractions of ISI cannot be excluded.

In summary, these comparisons of the data with the simulations confirm that there is substantial yield due to ISI, although 3N phase space appears to describe the larger part of the 3NA data. As the pion energy decreases, the indications of ISI weaken progressively, but nevertheless remain. Because of the strong qualitative features in the data, the existence of a significant ISI yield does not appear to be dependent on the models of the 3NA reaction used. However, the amount of ISI implied by the data may be model dependent.

The analysis presented here does not give an explanation of the origin of a large part of the 3NA yield. However, the magnitude of the clear ISI signal will be a useful constraint for quantum mechanical calculations of 3NA including full rescattering processes, and should clarify whether processes in addition to known interactions are necessary to explain this cross section.

6 Conclusion

Structures have been observed in the distributions of the protons emitted following the absorption of pions which indicate that part of the cross section is due to a two-step process (ISI) in which one proton is first knocked out by quasi-elastic pion scattering. These structures, in the proton angle and momentum distributions, and in the m_x^2 spectra, are clear signatures of this type of two-step process. Fits to the data suggest that this process accounts for 5 - 10% of the total absorption cross section, or up to one third of the three-nucleon yield. The fraction of ISI found in the data could be different if better physics models were used for the analysis. The larger part of three-nucleon absorption distributions may be described by a combination of phase space and distributions generated by simulations of quasi-free absorption followed by proton-proton rescattering (FSI), although the latter process does not appear to be strong.

We thank L. Canton, H. Kamada and M. Locher for useful discussions and the staff of the Paul Scherrer Institute for their considerable assistance in mounting and running this experiment. This work was supported in part by the German Bundesministerium für Forschung und Technologie, the German Internationales Büro der Kernforschungsanlage Jülich, the Swiss National Science Foundation, the US Department of Energy, and the US National Science Foundation.

References

[1] G. Backenstoss et al., Phys. Rev. Lett. 55 (1985) 2782.

[2] K.A. Aniol et al., Phys Rev C33 (1986) 1714.

[3] L.C. Smith et. al., Phys. Rev. C40 (1989) 1347.

[4] P. Weber et al., Nucl. Phys. A534 (1991) 541.

[5] S. Mukhopadhyay et al., Phys. Rev. C43 (1991) 957.

[6] T. Alteholz et al., Phys. Rev. Lett. 73 (1994) 1336.

[7] H.J. Weyer, Phys. Rep. 195 (1990) 295.

[8] C.H.Q. Ingram, Nucl. Phys. A553 (1993) 573c.

[9] N. d'Hose et al., Phys. Rev. Lett. 63 (1989) 856.

[10] A.J. Sarty et al., Phys. Rev. C47 (1993) 459.

[11] T. Emura et al., Phys. Rev. C49 (1994) R597.

[12] D.J. Tedeschi et al., Phys. Rev. Lett. 73 (1994) 408.

[13] G. Backenstoss et al., Phys. Lett. B222 (1989) 7.

[14] R.D. McKeown et al., Phys. Rev. 24 (1981) 211.

[15] J.P. Schiffer, Nucl. Phys. A335 (1980) 339.

[16] J.W. Negele and K. Yazaki, Phys. Rev. Lett. 47 (1981) 71.

[17] S. Fantoni, B.L. Friman and V.R. Pandharipande, Phys. Lett. 104B (1981) 89.

[18] G. Garino et. al., Phys Rev C45 (1992) 780.

[19] S.D. Hyman et al., Phys. Rev C47 (1993) 1184.

[20] K. Masutani and K. Yazaki, Nucl. Phys. A407 (1983) 309.

[21] E. Oset, Y. Futami and H. Toki, Nucl. Phys. A448 (1986) 597.

[22] W.J. Burger et al., Phys. Rev. Lett. 57 (1986) 58; Phys. Rev. C41 (1990) 22153.

[23] W. Brueckner et al., Nucl. Phys. A469 (1987) 617.

[24] R. Tacik et al., Phys. Rev. C40 (1989) 256.

[25] R. Ransome et al., Phys. Rev. C42, 1500 (1990); Phys. Rev. C46 (1992) 273.

[26] G. Backenstoss et al., Nucl. Inst. and Meth. A310 (1991) 518; T. Alteholz et al., submitted to Nucl. Inst. & Meth.; K.E. Wilson, PhD thesis, MIT, 1995.

[27] J. Köhler, PhD thesis, Univeristy of Basel, in preparation.

[28] N. Simicevic and A. Mateos, Phys. Rev. C51 (1995) 797.

[29] Y. Wu, S. Ishikawa and T. Sasakawa, Few Body Systems 15 (1993) 145; S. Ishikawa and Y. Wu, private communication, 1994.

[30] E. Jans et al., Phys Rev. Lett. 49 (1982) 974.

[31] B.G. Ritchie, Phys. Rev. C44 (1991) 533.

[32] SCATPI, J.B. Walter and G.A. Rebka, Los Alamos National Laboratory Report LA-7731-MS, 1979.

[33] R.A. Arndt et al., Phys. Rev. D32 (1985) 1085.

[34] L.L. Salcedo et al., Phys. Lett. B208 (1988) 339.

Figure captions

Fig. 1. The missing mass in the reaction ^{3}He(π^+,2p) at 118 MeV.

Fig. 2. The acceptance of LADS as a function of proton angle for the reaction π^{+3}He$\rightarrow$ 3p at 239 MeV, as determined from the weighted average of the results from the different simulations, for protons of more than 30 MeV energy.

Fig. 3. The distributions in momentum of the least energetic proton, corrected for the detector acceptance and divided by the 3N phase space. The distribution are arbitrarily normalised for each energy. The dots show the spectrum generated by the 2NA simulation for 118 MeV pions, normalised to the data according to the fits described in the text.

Fig. 4. For each incident pion energy, the correlation between proton angle and momentum for all detected events in which all protons were between 15° and 165° and had at least 30 MeV kinetic energy. The data are corrected for the detector acceptance. In the forward and backward regions, the protons with the highest kinematically allowed momenta fall outside the acceptance. The white lines indicate the kinematics of free π^+p scattering.

Fig. 5. The m_x^2 spectra (see text), for each incident pion energy. The cuts on and corrections to the data are the same as those for Fig. 4. Also shown are the distributions from the simulations (2NA, FSI, ISI and phase space) and their sum, normalised from the fit to the data.

Fig. 6. The correlation between m_x^2 and proton momentum (upper) and proton angle (lower), for 239 MeV incident pions, with the same cuts on and corrections to the data as for Figs 4 and 5. The contours indicate the locations of the peaks due to 2NA, which has been suppressed by the 30 MeV minimum energy requirement.

[20] K. Masutani and K. Yazaki, Nucl. Phys. A407 (1983) 309.

[21] E. Oset, Y. Futami and H. Toki, Nucl. Phys. A448 (1986) 597.

[22] W.J. Burger et al., Phys. Rev. Lett. 57 (1986) 58; Phys. Rev. C41 (1990) 22153.

[23] W. Brueckner et al., Nucl. Phys. A469 (1987) 617.

[24] R. Tacik et al., Phys. Rev. C40 (1989) 256.

[25] R. Ransome et al., Phys. Rev. C42, 1500 (1990); Phys. Rev. C46 (1992) 273.

[26] G. Backenstoss et al., Nucl. Inst. and Meth. A310 (1991) 518; T. Alteholz et al., submitted to Nucl. Inst. & Meth.; K.E. Wilson, PhD thesis, MIT, 1995.

[27] J. Köhler, PhD thesis, Univeristy of Basel, in preparation.

[28] N. Simicevic and A. Mateos, Phys. Rev. C51 (1995) 797.

[29] Y. Wu, S. Ishikawa and T. Sasakawa, Few Body Systems 15 (1993) 145; S. Ishikawa and Y. Wu, private communication, 1994.

[30] E. Jans et al., Phys Rev. Lett. 49 (1982) 974.

[31] B.G. Ritchie, Phys. Rev. C44 (1991) 533.

[32] SCATPI, J.B. Walter and G.A. Rebka, Los Alamos National Laboratory Report LA-7731-MS, 1979.

[33] R.A. Arndt et al., Phys. Rev. D32 (1985) 1085.

[34] L.L. Salcedo et al., Phys. Lett. B208 (1988) 339.

Figure captions

Fig. 1. The missing mass in the reaction ^{3}He(π^+,2p) at 118 MeV.

Fig. 2. The acceptance of LADS as a function of proton angle for the reaction π^{+3}He$\rightarrow$ 3p at 239 MeV, as determined from the weighted average of the results from the different simulations, for protons of more than 30 MeV energy.

Fig. 3. The distributions in momentum of the least energetic proton, corrected for the detector acceptance and divided by the 3N phase space. The distribution are arbitrarily normalised for each energy. The dots show the spectrum generated by the 2NA simulation for 118 MeV pions, normalised to the data according to the fits described in the text.

Fig. 4. For each incident pion energy, the correlation between proton angle and momentum for all detected events in which all protons were between 15° and 165° and had at least 30 MeV kinetic energy. The data are corrected for the detector acceptance. In the forward and backward regions, the protons with the highest kinematically allowed momenta fall outside the acceptance. The white lines indicate the kinematics of free π^+p scattering.

Fig. 5. The m_x^2 spectra (see text), for each incident pion energy. The cuts on and corrections to the data are the same as those for Fig. 4. Also shown are the distributions from the simulations (2NA, FSI, ISI and phase space) and their sum, normalised from the fit to the data.

Fig. 6. The correlation between m_x^2 and proton momentum (upper) and proton angle (lower), for 239 MeV incident pions, with the same cuts on and corrections to the data as for Figs 4 and 5. The contours indicate the locations of the peaks due to 2NA, which has been suppressed by the 30 MeV minimum energy requirement.

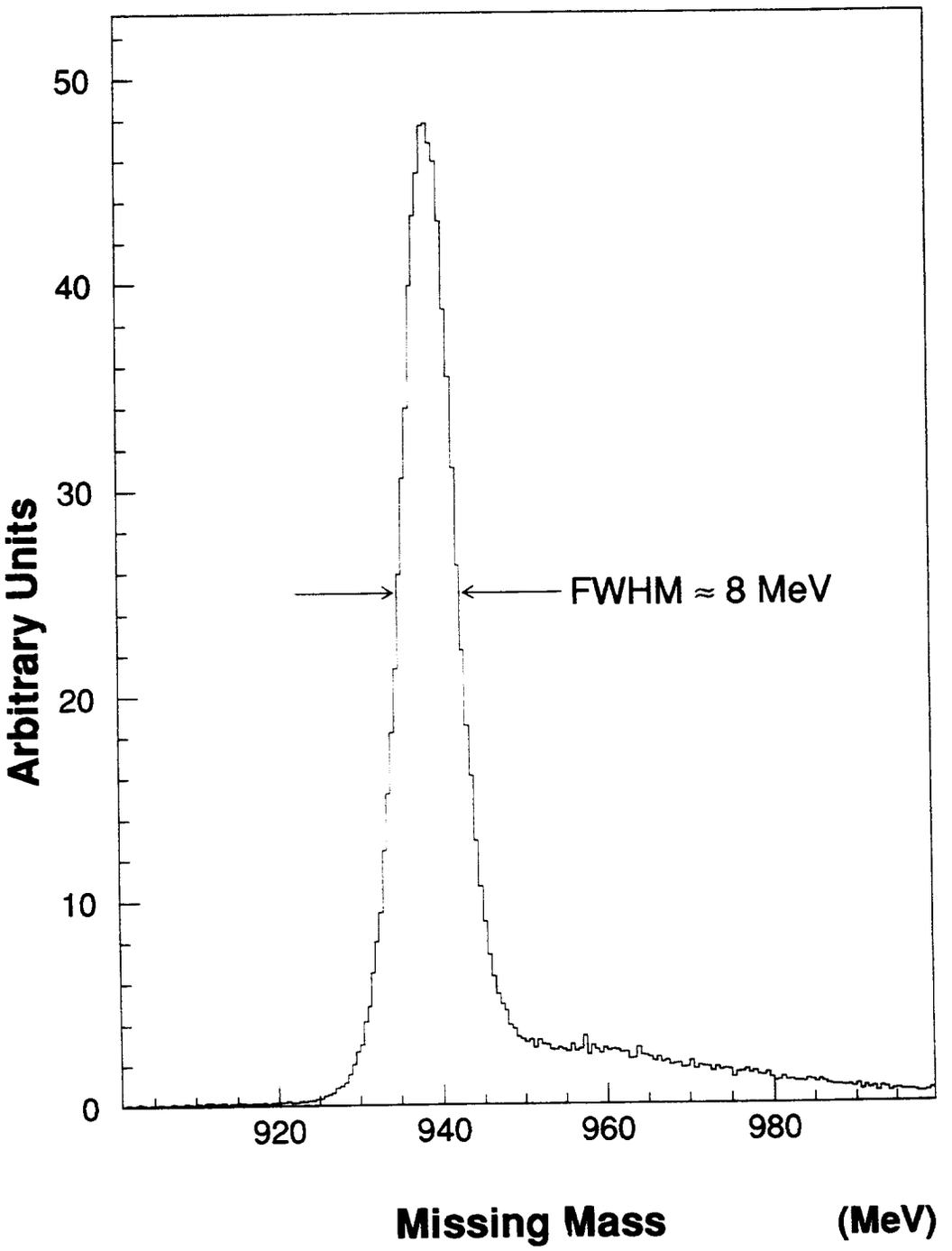
50
40
30
20
10
0
Arbitrary Units
FWHM ≈ 8 MeV
920
940
960
980
Missing Mass
(MeV)

Fig 1

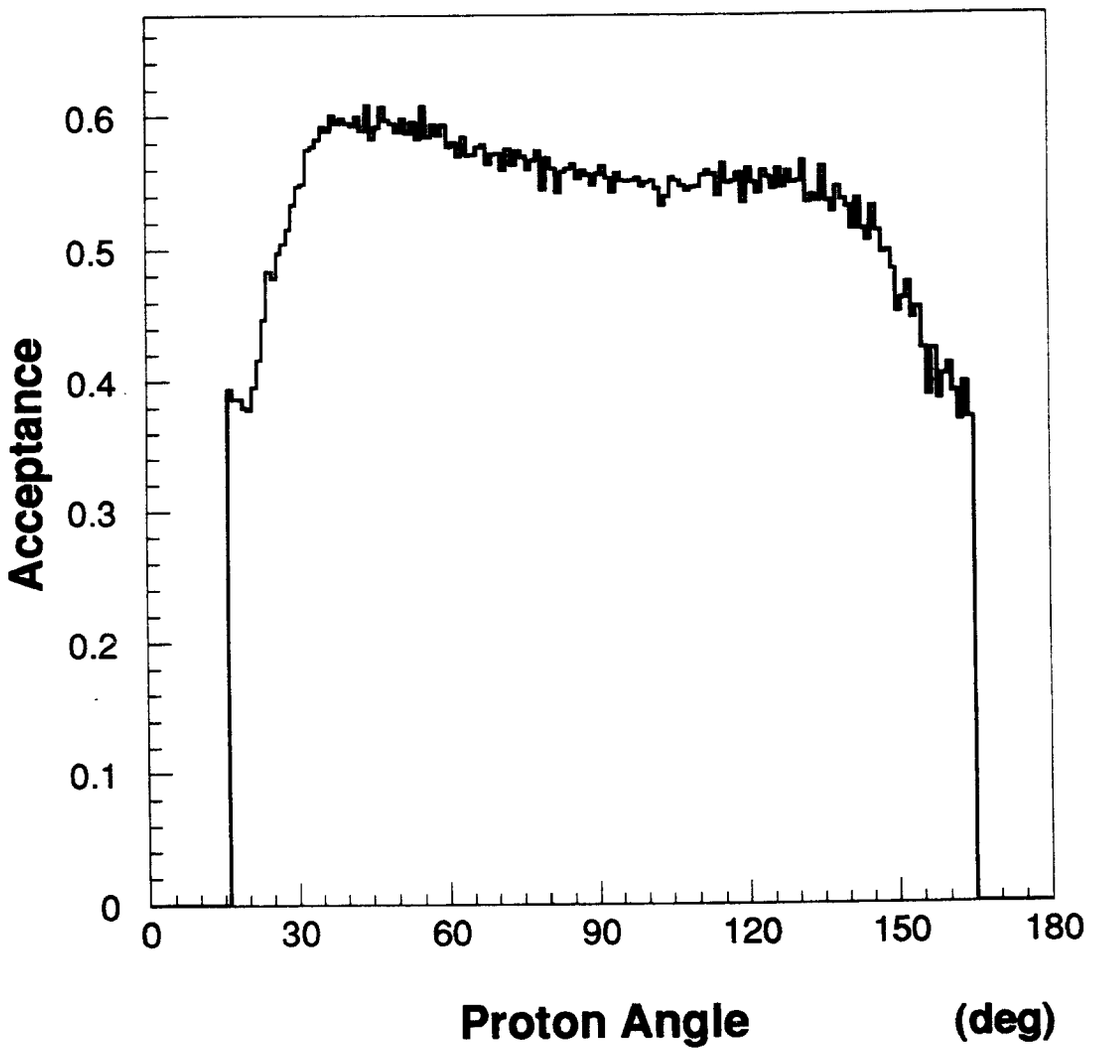
Acceptance
0.6
0.5
0.4
0.3
0.2
0.1
0
0
30
60
90
120
150
180
Proton Angle
(deg)

Fig 2

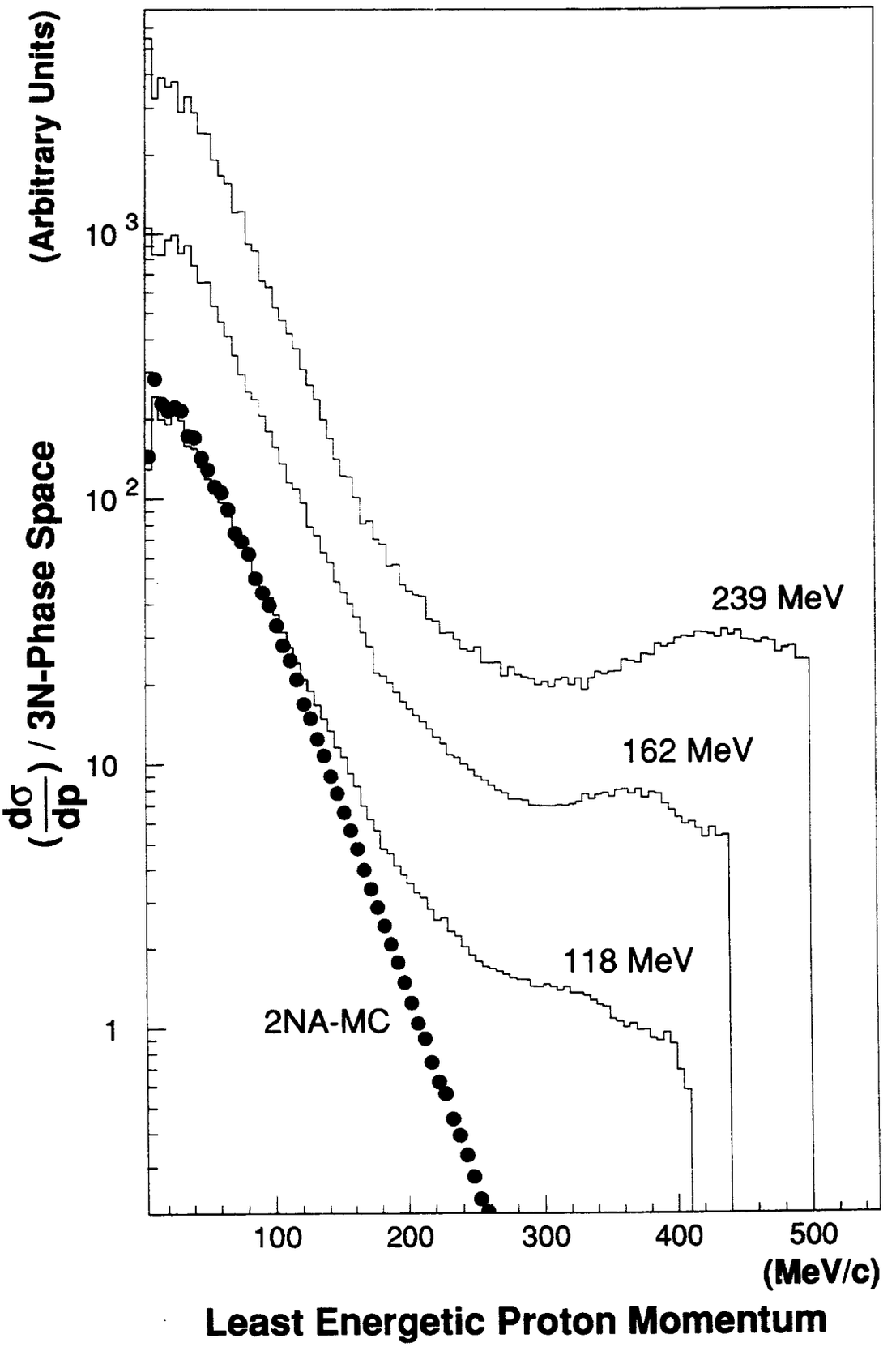
(Arbitrary Units)
$(\frac{d\sigma}{dp})$ / 3N-Phase Space
10^3
10^2
10
1
239 MeV
162 MeV
118 MeV
2NA-MC
100
200
300
400
500
(MeV/c)
Least Energetic Proton Momentum

Fig 7

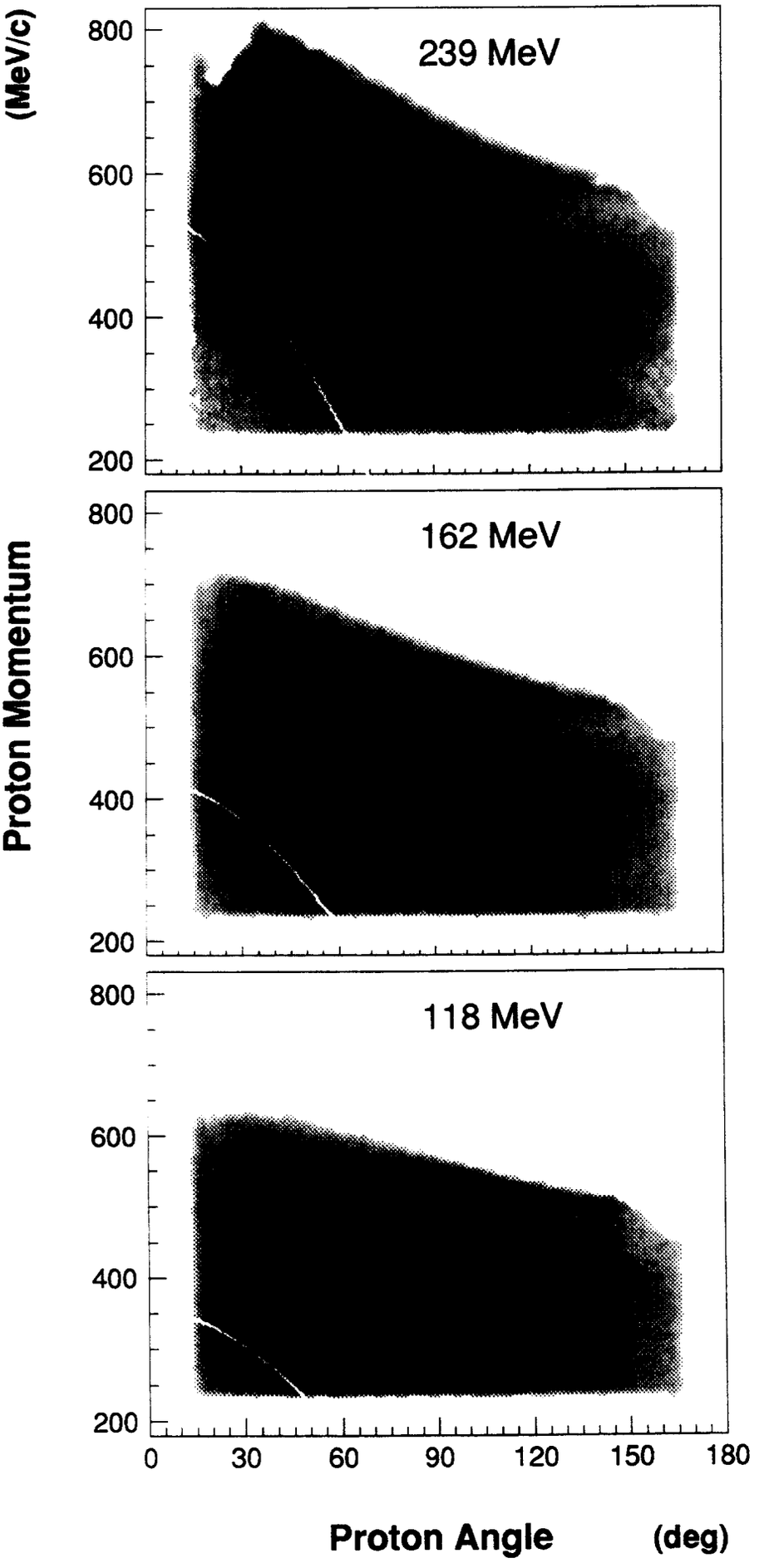
239 MeV
162 MeV
118 MeV
800
600
400
200
0
30
60
90
120
150
180
Proton Momentum
(MeV/c)
Proton Angle
(deg)

Fig. 6

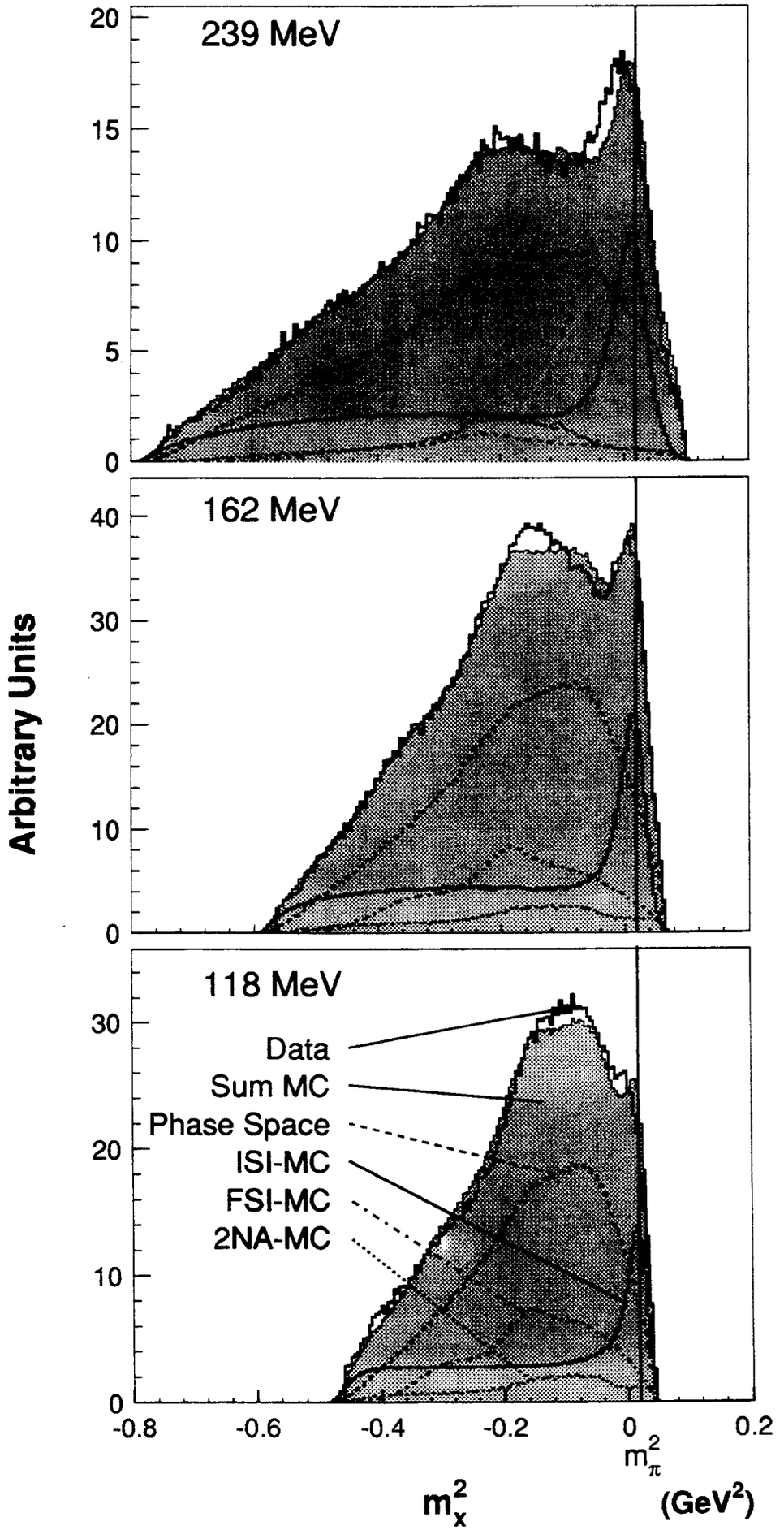
239 MeV
162 MeV
118 MeV
Data
Sum MC
Phase Space
ISI-MC
FSI-MC
2NA-MC
Arbitrary Units
m_x^2 (GeV^2)
m_π^2

Fig 5

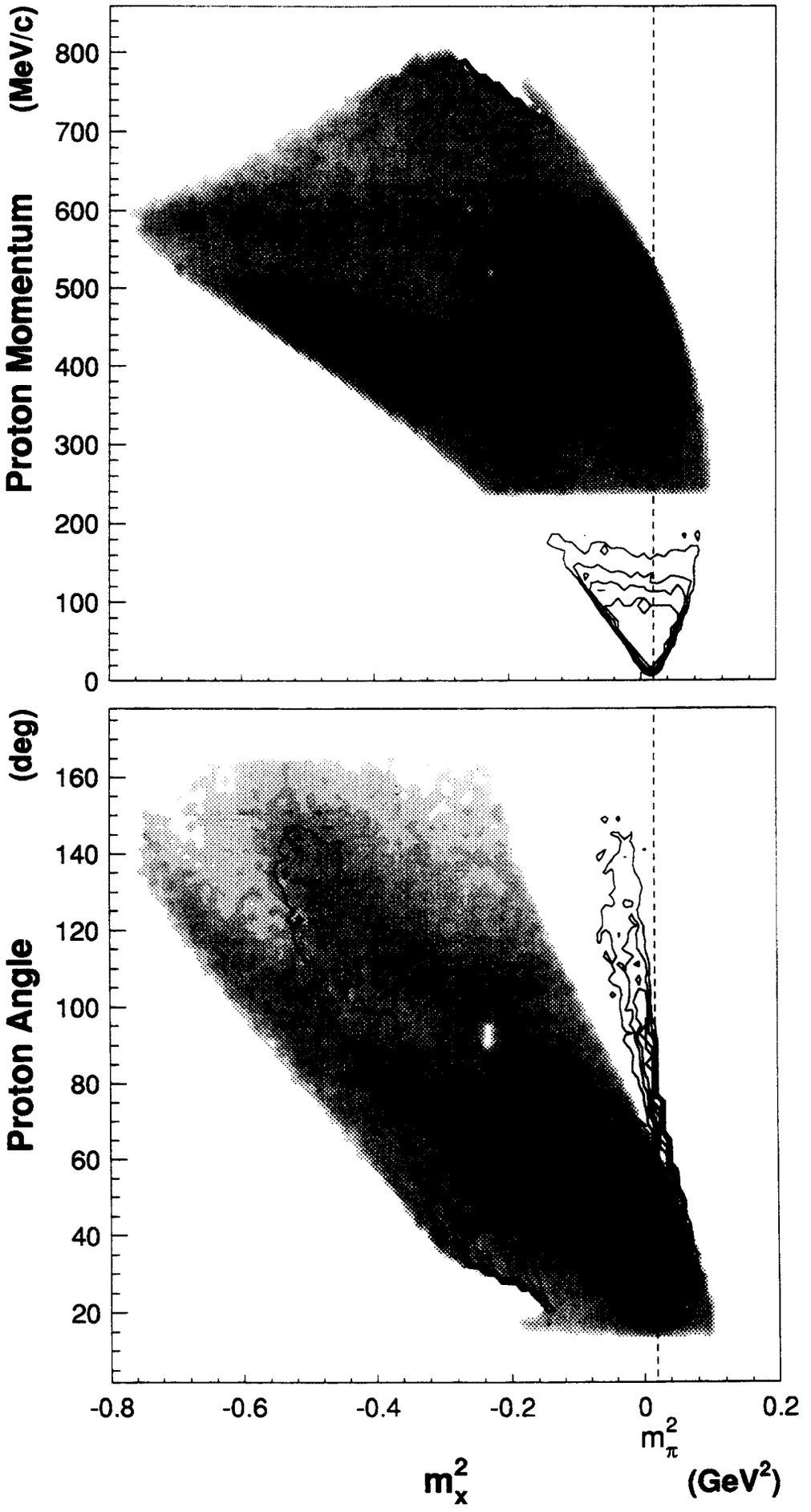
Proton Momentum (MeV/c)
800
700
600
500
400
300
200
100
0
Proton Angle (deg)
160
140
120
100
80
60
40
20
-0.8
-0.6
-0.4
-0.2
0
0.2
m_π^2
m_x^2 (GeV^2)

Fig 6